Institut für Photovoltaik

Institute for Photovoltaics

Universität Stuttgart

Jahresbericht

Annual Report 2012

Jahresbericht
Annual Report 2012

Redaktion • edited by:

Anja Hardekopf
Jürgen R. Köhler
Jürgen H. Werner
grafik-service@web.de

Vorwort

Liebe Freunde des *ipv*,

das Institut hat mit dem neuen Namen „für Photovoltaik“ das erste Jahr hinter sich gebracht - mitten in der viel diskutierten Energiewende. Wenn man über die letzten 30 Jahre Entwicklung zurück blickt, ist es erstaunlich zu sehen, wie die Photovoltaik sich von Kleinstanwendungen für Taschenrechner, Armbanduhren und Kinderspielzeug bis zu einer Leistung von 30 GW im deutschen Stromnetz entwickelt hat. Auch das Wettrennen der Technologien ist faktisch längst entschieden: Kristallines Silizium hat sich - wie in der Mikroelektronik - durchgesetzt. Für die restlichen Technologien bleiben hart umkämpfte Nischenmärkte.

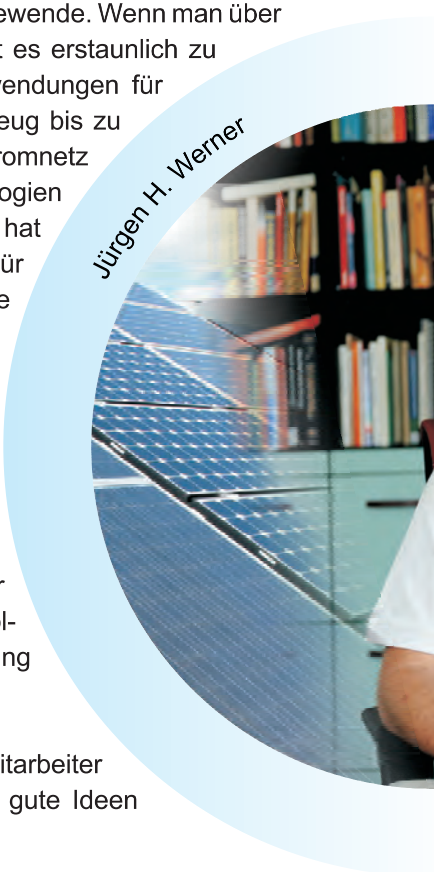

Forschung und Lehre im Bereich Photovoltaik ist notwendiger denn je, aber sie wird sich verlagern: Von der Technologie der Zellen hin zur Systemtechnik, Betriebsführung, Überwachung und Diagnose von Anlagen, Netzeinbindung und Speicherung von elektrischem Strom. Kurz: von der Halbleitertechnologie zur „Intelligenz“ in Photovoltaikanlagen. Das *ipv* ist für diese Herausforderung gerüstet.

Ich bin mir sicher, dass die Mitarbeiterinnen und Mitarbeiter des *ipv* auch in der dynamischen Energiewende gute Ideen entwickeln können und werden.

Stuttgart, Dezember 2012

J. Werner

Jürgen H. Werner

Preface

Dear friends of the *ipv*,

after the first year with the new name "for Photovoltaics" the institute is in the middle of the German struggle for the energy turn around. Within the last 30 years, photovoltaics went through an astonishing development. It started from a technology for pocket calculators, wrist watches and toys to the present status with 30 GW photovoltaic power installed in Germany alone. Also, the rat race of technologies is *de facto* decided: Similarly to microelectronics, crystalline silicon darwinistically dominates also PV. All other technologies fight hard in and for niche markets.

In these times, research and education in the field of photovoltaics is important more than ever before. However, the *foci* shift: From cell technology to systems, their control, surveillance and diagnosis, grid integration and storage of electricity. In short: from semiconductor technology to "intelligence" in photovoltaic systems. The *ipv* is aware of and ready for this challenge.

I am confident that the people within the *ipv* will continue to develop bright ideas in the dynamic time of the energy turn around.

Stuttgart, December 2012

J. Werner

Jürgen H. Werner

Inhaltsverzeichnis • Table of Contents

Mitarbeiter
People

Forschung

Solarzellen

Photovoltaik-Systeme

Mikro - und Optoelektronik

Energie

Lehre

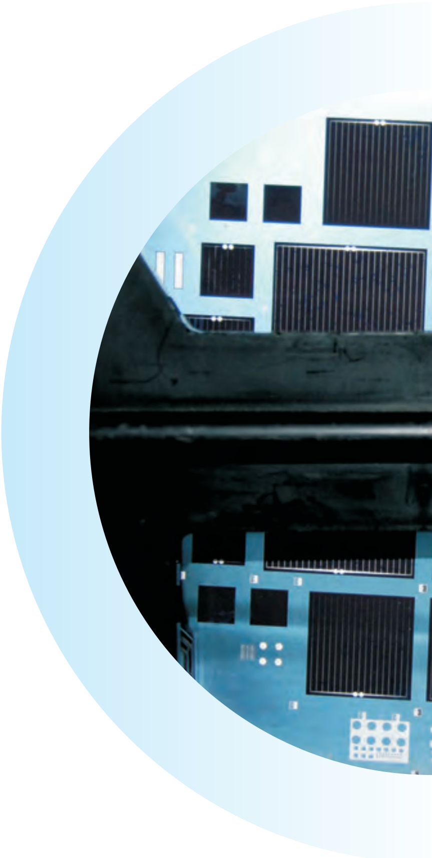

Institutsleitung • Head of the Institute

Verwaltung • Administration

Gruppe Laserprozesse
Group Laser Processing

(Gruppenleiter / Group Leader: Jürgen R. Köhler)

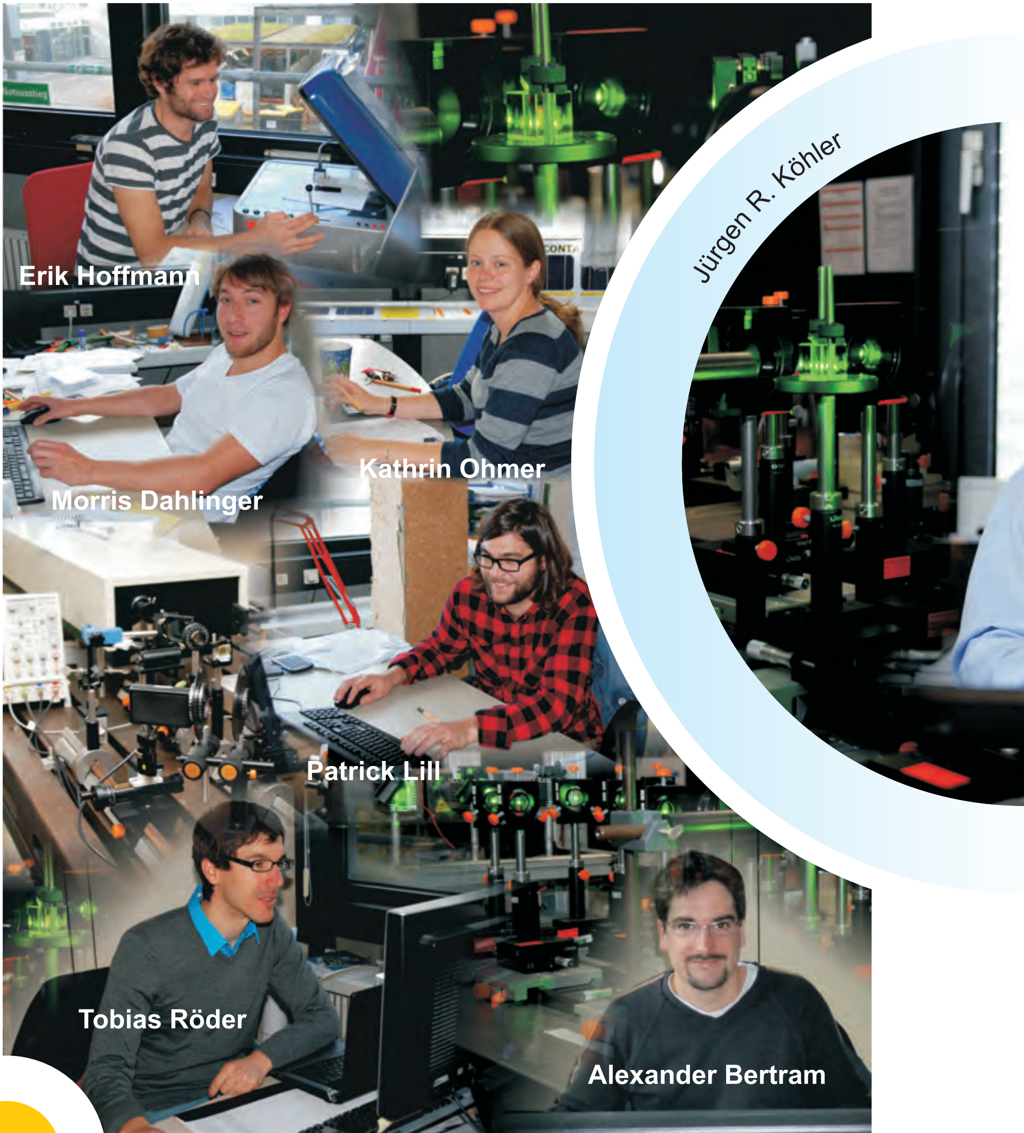

Die Gruppe „Laserprozesse“ entwickelt neue Technologien zum Laserprozessieren einkristalliner und multikristalliner Silizium-Scheiben. Hierzu zählen die laserunterstützte Abscheidung von Metallkontakten, die Erzeugung von Lasergräben für vergrabene Siebdruckkontakte, die Kantenisolierung von Solarzellen sowie die Laser-Dotierung zur Herstellung von ganzflächigen und selektiven Dotierungen für Vorderseiten- und Rückseiten-kontaktierte Zellen. Im Vordergrund unserer Arbeiten stehen Grundlagenuntersuchungen zur Laserdotierung sowie zur laserunterstützten Feinlinienmetallisierung. Entwicklungsziele sind die Erhöhung des Durchsatzes bei der laserunterstützten Emitterdotierung sowie die Steigerung der Wirkungsgrade von bis zu 156 mm x 156 mm großen einkristallinen und multikristallinen Silizium-Solarzellen Richtung 20 %. In enger Zusammenarbeit mit der Gruppe „Industrielle Solarzellen“ am *ipv* optimieren wir unsere Laserprozesse zusammen mit der Siebdrucktechnik zur Herstellung hocheffizienter, industrietauglicher Solarzellen.

The “laser processing” group explores new technologies for laser processing of mono- and multi-crystalline silicon wafers. Examples are laser assisted metal deposition, laser grooved buried screen printed contacts, laser edge isolation, as well as selective laser doping for front and rear side contacted crystalline silicon solar cells. The main topic of our research work is the investigation of the fundamental processes involved in pulsed laser doping as well as in laser assisted fine line metallization of crystalline silicon wafers. Development goals are the increase of the throughput rate of the laser doping process as well as the increase of the efficiency of up to 156 mm x 156 mm sized mono- and multi-crystalline silicon solar cells up to 20 %. A close collaboration with the “industrial solar cells group” at *ipv* optimizes our laser processing technology together with screen printing technology for high efficiency industrial cells.

Gruppe Technologie
Group Technology

(Gruppenleiterin / Group Leader: Birgitt Winter)

Die Gruppe „Technologie“ setzt sich aus den technischen Mitarbeitern des Instituts zusammen. In ihr ist die gesamte Institutsinfrastruktur in einer Gruppe zusammengefasst. Diese Vernetzung von Experten im technischen Bereich ermöglicht eine gute Koordinierung aller anfallenden Arbeiten, sei es bei Routineanalysen, Optimierung von Messaufbauten, Laborumbaumaßnahmen und vor allem bei der Weiterentwicklung wichtiger Technologien. Dazu gehören Oxidationen, Diffusionen, Plasmadepositionen, nasschemische Reinigung und Ätzen, Lithographie, Metallisierung und vieles andere mehr. Unser Ziel ist eine gute Reproduzierbarkeit von Prozessen durch die Entwicklung von standardisierten Prozessabläufen und Qualitätskontrollstandards. Diese Vorgehensweise bietet uns eine gute Basis, um gleichzeitig auch immer auf neue Anforderungen zu reagieren, die durch laufende Projekte am *ipv* erwachsen.

The group “Technology” pools all technical assistants and engineers of the institute. The whole infrastructure of the institute is combined in one group. The cross linking of technical experts allows an effective coordination of the requested demands. We make standard analyses, upgrade measurement setups, coordinate the reconstruction of the laboratory and mainly enhance technical processes. The processes include oxidations, diffusions, plasma enhanced depositions, wet chemical cleaning and etching, lithography and metallization. Our aim is a high reproducibility of all processes by developing standardized procedures. This is the basis to react to new demands that grow within running projects at *ipv*.

Gruppe Dünnschichtsilizium
Group Thin Film Silicon

(Gruppenleiter / Group Leader: Markus Schubert)

Die Arbeitsgruppe „Dünnschichtsilizium” entwickelt Solarzellen und Photodetektoren auf der Basis amorphen und nanokristallinen Siliziums. Die *in-situ* Serienverschaltung vereinfacht die Herstellung flexibler Photovoltaikmodule. Eine Mikrowellenquelle erlaubt schnelle Plasmaabscheidungen von nanokristallinem Silizium für gestapelte Dünnschichtsolarzellen. Ultradünne amorphe Siliziumschichten dienen der Passivierung und Verbesserung kristalliner Siliziumsolarzellen. Spezielle Dünnschicht-Photodetektoren quantifizieren Herzinfarkt-, Tumor- und Entzündungsmarker in einem mobilen Gerät für Point-of-Care Diagnostik. In enger Zusammenarbeit mit dem Institut für Physikalische und Theoretische Chemie der Universität Tübingen und europäischen Partnern entwickeln wir ein mobiles Messgerät zur Überwachung der Medikamentierung von Patienten nach Organtransplantionen.

The “Thin Film Silicon” work group at *ipv* is developing solar cells and photodetectors based on amorphous and nanocrystalline silicon thin films. The *in-situ* series connection facilitates manufacturing of flexible photovoltaic modules. A microwave source enables fast plasma deposition of nanocrystalline silicon for thin film tandem solar cells. Ultrathin amorphous silicon layers passivate and improve crystalline silicon solar cells. Application specific thin film photodetectors quantify heart attack, cancer and inflammation markers in a mobile point-of-care device. In close cooperation with the Department of Analytical Chemistry at the Eberhard Karls University of Tübingen and European partners we develop a mobile setup for therapeutic drug monitoring in patients after organ transplantation.

Gruppe Industrielle Solarzellen
Group Industrial Solar Cells

(Gruppenleiterin / Group Leader: Renate Zapf-Gottwick)

Die Gruppe „Industrielle Solarzellen” zielt mit ihren Forschungsaktivitäten auf industrienahe Prozesse, die den Wirkungsgrad von kristallinen Silizium-Solarzellen verbessern und ihre Herstellungskosten verringern. Unsere stabile „Baseline” auf hohem Wirkungsgradniveau als Referenz zeigt, dass innovative Prozesse das Potential haben, den Wirkungsgrad noch zu steigern. Wir arbeiten, auch zusammen mit den anderen *ipv*-Gruppen, an „Add-on”- Prozessen: der Kontaktierung von hochohmigen Emittern mit und ohne laserdotiertem selektivem Emitter, dem Feinlinien-Siebdruck der Vorderseitenmetallisierung, dem Ersetzen von Silber, als einem kostenintensiven Teil in der Solarzellenprozessierung durch andere Materialien, aber auch an Alternativen zur Aluminium-Rückseite. Ein weiterer Ansatz ist die Optimierung auf Modulebene. Hier zeigt sich großes Potential in der Verringerung der optischen Verluste mit Hilfe des Prinzips der Totalreflexion.

Our group “industrial solar cells” is engaged in different research activities for higher efficiencies and less production costs of solar cells in industry oriented processes. Our stable “baseline” on a high efficiency level as a reference shows that innovative processes have still a great potential for boosting the efficiency. We work together with the other *ipv*-groups on add-on processes such as contacting of high ohmic emitters with and without laser-doped selective emitters, fine-line screen printing of the front side metallization, the replacement of silver, which is a cost-intensive part in solar cell processing, by other materials and also on alternatives to the aluminium back side. The optimization of solar modules is also important. Here we are working on the decrease of optical losses by activating optical inactive parts of modules.

Gruppe Charakterisierung
Group Characterization

(Gruppenleiter / Group Leader: Markus Schubert)

Die Arbeitsgruppe „Charakterisierung" konzentriert sich auf die Analyse und Modellierung von Photovoltaikmaterialien und Halbleiterbauelementen, insbesondere Solarzellen, sowie von PV-Modulen und -Systemen. Dazu untersuchen wir strukturelle, chemische, optische und elektrische Eigenschaften von Einzelschichten und Bauelementen, wie Ladungsträgerlebensdauer, Strom/Spannungscharakteristik, Spektralempfindlichkeit, ortsaufgelöste Kurzschlussstromdichte, Elektro- und Photolumineszenz. Innovative optische Konzepte zielen auf die Steigerung des Wirkungsgrades von Solarzellen und PV-Modulen. Die langjährige Aufzeichnung von Betriebsparametern und Energieertrag, neuartige Analysemethoden wie Lumineszenzbilder bei Tageslicht und deren modellhafte Beschreibung erleichtern die Fehlersuche in PV-Anlagen und deren Optimierung.

The "Device Analysis" group focuses on analyses and modelling of photovoltaic materials and semiconductor devices, especially of solar cells, as well as photovoltaic modules and systems. We investigate structural, chemical, optical and electrical properties of single layers and devices, such as charge carrier lifetime, current-voltage characteristics, spectral response, spatially resolved short circuit current density, electro- and photoluminescence. Innovative optical concepts aim at enhancing the conversion efficiency of solar cells and modules. The long-year recording of operating parameters and energy yield, novel characterization methods like daylight luminescence mapping and corresponding mathematical modelling facilitate fault detection and optimization of photovoltaic systems.

einkristallines

mikrokristallines

Silizium

nanokristallines

amorphes

Wissenschaftliche Beiträge
Scientific Contributions

2

Publikationen
Publications

Screen Printed Laser Grooved Buried Contacts

Author: A. Bertram
In collaboration with: M. Saueressig and J. R. Köhler

Cost reduction and efficiency gain are the main objectives for improved solar cell processing. Combining laser processed fine line grooves and standard screen printing technology reduces the front side shading and allows the use of high ohmic emitters by increasing the contact area of the contact fingers. In addition, silver consumption is reduced.

Our simple and cost effective laser ablation process enables processing of 70 μm wide and 40 μm deep grooves for subsequent screen printing. Solar cell processing in Fig. 1 starts with the laser ablation. Damage etching and alkaline surface texturing remove the laser damage. The U-shaped laser grooves increase the contact area of the contact fingers by a factor 1.8, allowing to increase the furnace diffused emitter sheet resistance from 60 W/sq to 80 W/sq without increasing the contact resistance. A finger aspect ratio *AR* > 0.5 results in negligible mesh marking and reduces the silver consumption for the front side metallization by 30 %. Compared to other buried contact metallization processes [1] our process does not require any addition chemical etching or cleaning.

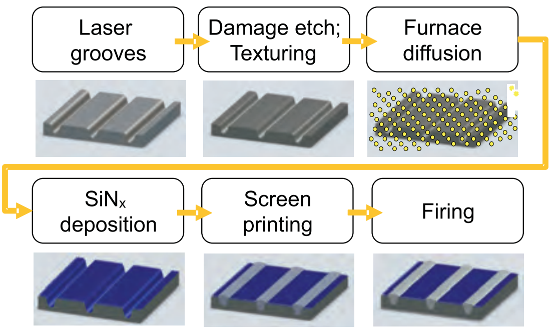

Figure 1:
Processing of laser grooved cells.

Our process is compatible with standard screen printing technology. Figures 2 and 3 present the grooves before and after screen printing. The grooves have a U-shaped structure, which ensures the printability of standard screen printing pastes.

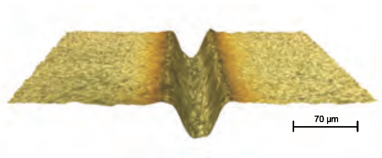

Figure 2:
Laser groove with optimized parameters for screen printing.

Figure 3:
Screen printed buried contact with 70 µm wide finger.

Table I compares the best screen printed laser grooved buried contacts with the best standard solar cell. The standard cell has 70×110 µm wide and 25 µm high contact fingers, whereas the buried contact cell uses 90×70 µm wide and 40 µm deep fingers. Both cells have two 2 mm wide bus bars. The smaller fingers reduce front side shading from 7.5 % to 6.6 % and increase the short circuit current density by ΔJ_{SC} = 0.4 mA/cm^2. The 80 Ω/sq emitter improves the blue response resulting in an additional current density gain ΔJ_{SC} = 0.9 mA/cm^2. The reduced saturation current density of the emitter increases the open circuit voltage by ΔV_{OC} = 13 mV. The solar cell efficiency increases by $\Delta\eta$ = 0.8 % absolute.

Table I: Solar cell results measured with a Halm-flasher

Cell	V_{OC} (mV)	J_{SC} (mA/cm^2)	*FF* (%)	η (%)
Buried contact	632	37.2	78.2	18.4
Reference	619	35.9	79.1	17.6

References:

[1] M. Green and S. Wenham 1984, IP Australia, patent application number 1984036664.

Optimization of the Phosphorus Diffusion for Laser Doping

Author: B. Bazer-Bachi
In collaboration with: M. Dahlinger and R. Zapf-Gottwick

Advanced structures in solar cells, such as selective emitter or back contacted back junction solar cells, require different phosphorus doping levels. We pursue a trade-off between the low Auger recombination due to lowly doped regions and the low contact resistance due to a sufficient phosphorus concentration under the metallization.

A phosphorus furnace diffusion creates the lowly doped region, needed for a high carrier lifetime between the contacts. The phosphosilicate glass deposited during the diffusion serves as a precursor layer for laser doping. We introduce an additional step during the diffusion, named preoxidation, prior to the introduction of the dopant source. The preoxidation leads to the growth of a thin oxide layer which consumes part of the inactive phosphorus atoms during the following diffusion [1]. The ratio between the precursor's gases, i.e. $POCl_3$ and O_2, is also varied in order to change the phosphorus concentration in the PSG. A part of the samples undergoes the *ipv*-laser doping process. Both furnace diffused and laser doped phosphorus layers then receive a thermal oxidation at 1000°C for 1 hour, in order to passivate the surface.

Table I shows the effect of the preoxidation time on sheet resistance R_{sh} and saturation current J_{0s}. For increasing t_{preox}, the “preoxide” thickness grows and this part of the P-profile is lost during PSG etching. Then, the sheet resistance R_{sh} increases and Auger recombination is reduced. The saturation current density J_{0s} decreases to J_{0s} = 10 fA/cm^2 for t_{preox} = 60 min. However, preoxidation limits the laser doping. Therefore, we change the $POCl_3/O_2$ ratio to increase the phosphorus “reservoir” for laser doping, i.e. the P-concentration in the PSG. By increasing the $POCl_3/O_2$ ratio, the sheet resistance after laser doping is R_{LD} = 47 Ω/sq for $POCl_3/O_2$ = 6 instead of R_{LD} = 76 Ω/sq for $POCl_3/O_2$ = 3.75.

Table I: Influence of preoxidation time t_{preox} and $POCl_3/O_2$ ratio on sheet resistance R_{sh} and saturation current density J_{0s}. R_{sh} are shown after oxidation on diffused samples (R_{sh}) and on laser doped samples (R_{LD}). J_{0s} is measured on diffused samples after oxidation. Laser pulse energy H_P is fixed to H_P = 2.25 J/cm^2.

t_{preox} [min.]	$POCl_3/O_2$ ratio	R_{sh} [Ω/sq]	J_{0s} [fA/cm^2]	R_{LD} [Ω/sq]	ρ_c [mΩcm^2]
0	3.75	57	48	29	1.6
30	3.75	125	21	56	6.8
60	3.75	297	10	76	9.8
60	6	187	12	47	5.7

Table I also shows the changes in contact resistance ρ_c for three different t_{preox} and two different $POCl_3/O_2$ ratios. By increasing the preoxidation time from t_{preox} = 0 min to t_{preox} = 60 min, the contact resistivity dramatically increases from ρ_c = 1.6 mΩcm^2 to ρ_c = 9.8 mΩcm^2, due to higher R_{LD}. By increasing the $POCl_3/O_2$ ratio from 3.75 to 6, the contact resistivity reduces from to ρ_c = 5.7 mΩcm^2, as R_{LD} is reduced, thanks to the higher content of phosphorus in PSG.

The trade-off between preoxidation with low J_{0s} = 12 fA/cm^2 and a high higher P-content in PSG for laser doping with ρ_c = 5.7 mΩcm^2 allows excellent surface passivation and a low contact resistance.

References:

[1] B. Bazer-Bachi, P. Lill, M. Dahlinger, S. J. Eisele, R. Zapf-Gottwick, J. R. Köhler, and J. H. Werner, *Proc.27th EU PVSEC, 1954 (2012)*

Self-Doping Laser Transferred Contacts for c-Si Solar Cells

Author: E. Hoffmann
In collaboration with: T. C. Röder and J. R. Köhler

Laser transferred contacts with Ni, introduced by Röder et al [1], provide fine line silver free front side metallization fingers. Here, we use the metal antimony, Sb. In this case, the contacts simultaneously form a self-aligned n-type selective emitter and contact the front side of the cell. The Sb doped contacts subsequently act as seed layer for nickel and copper plating, resulting in a fine line front metallization with finger width w_F = 20 µm, contact resistivity as low as ρ_c = 2.0 mΩcm^2, and metallization resistivity ρ_M = 2.0××10^{-6} Ωcm. First solar cells show an efficiency η = 17.5 %.

Figure 1 shows the principle of the process. A pulsed green laser irradiates a one side antimony coated transparent support. The irradiation ablates the Sb and melts the underlying silicon. The transferred Sb diffuses into the silicon melt. Upon termination of the laser pulse, the silicon re-crystallizes epitaxially, incorporating the Sb atoms and forming a highly n-type doped selective emitter.

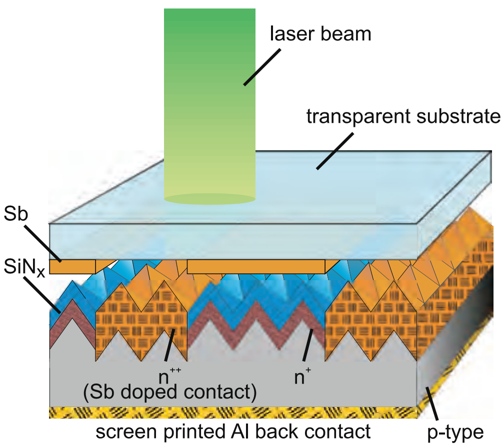

Figure 1:
Contact and selective emitter formation by laser induced forward transfer. A pulsed laser beam irradiates a transparent antimony coated substrate. The Sb melts and transfers through the SiN$_X$ anti-reflective coating. Additionally, the laser beam melts the silicon surface allowing the Sb to diffuse into the silicon melt. After epitaxial recrystallization the irradiated area is highly doped and enables an ohmic contact to the n-type emitter.

Figure 2 a) shows sheet resistance measurements of a textured p-type 3 Ωcm wafer after full area transfer of 130 nm Sb. With higher laser pulse energy density and more irradiation cycles the sheet resistance decreases as more Sb diffuses deeper into the wafer. However, with irradiation cycles $N_I > 10$, the sheet resistance starts to increase, indicating an out-diffusion of the incorporated Sb. The contact resistivity shown in Fig. 2 b) also decreases with increasing laser pulse energy density and irradiation cycles. Higher doping concentration enables contact resistivities as low as ρ_c = 2.0 mΩcm^2.

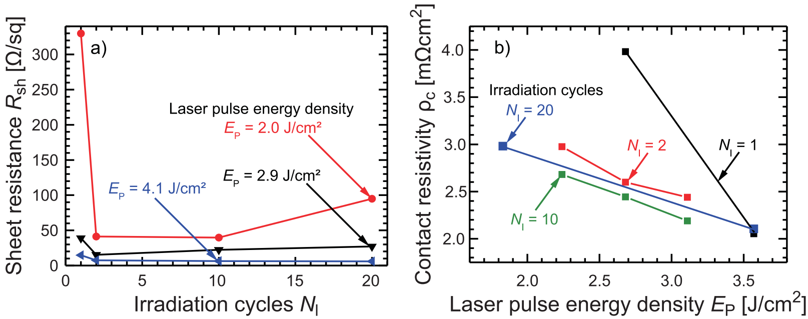

Figure 2:
a) Sheet resistance after Sb transfer dependson irradiation cycles N_I. A minimum between $5 < N_I < 10$ indicates a depletion of the Sb source after repeated irradiation. b) Contact resistivity ρ_c decreases with rising laser pulse energy density E_P. Increasing the irradiation cycles leads to improved contact resistivity. However, for $N_I > 10$ the contact resistivity starts to increase.

Solar cells achieve an efficiency η = 17.5 % on an area A = 4 cm^2. Due to the low finger width w = 20 µm, the short circuit current reaches J_{SC} = 39.5 mA/cm^2. Cell efficiency is limited by open circuit voltage V_{SC} = 603 mV and fill factor FF = 76.3 %. After grid optimization and improved cell processing we expect efficiencies η > 19 %.

References:

[1] T. C. Röder, E. Hoffmann, J. R. Köhler, and J. H. Werner, *Proc. 35th IEEE PVSC, 3597 (2010).*

Metallization of Back-Contacted Silicon Solar Cells

Author: G. Kulushich
In collaboration with: R. Zapf-Gottwick

The present work applies an analytical method to optimize the metallization design of our laser processed back-contact back-junction (BCBJ) solar cell developed at *ipv* [1]. First, a numerical simulator calculates the efficiency η, the short circuit current density J_{sc}, the open circuit voltage V_{oc}, and the fill factor *FF* for different pitch *p*, for a cell without metallization losses. Then, by taking into account the line resistance loss due to the emitter and BSF fingers, an analytical model assesses the influence of the emitter finger width $w_{f,em}$ and the BSF finger width $w_{f,BSF}$ on η and *FF*. The combination of numerical device simulation and analytical cell simulation, predicts a maximal efficiency η = 23.4 % on 6” cell size, for a pitch *p* = 1200 µm and a realistic case of Ag screen printed fingers with resistivity ρ = 5 µΩcm.

Figure 1 illustrates the back side structure of the BCBJ solar cell with an area *L* × *L* used for simulating the influence of the finger line resistance losses. The cell has two bus bars of width w_{bb}, one collecting the current from the emitter fingers and the second one collecting the current from the contact fingers to the base. Between the metallization of the emitter and the BSF there is an isolation layer of width w_i.

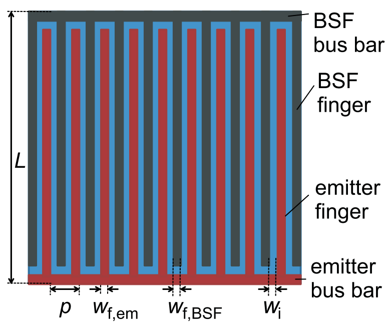

Figure 1:
Schematic top view of the back side of a BCBJ solar cell of length *L*. The cell has two bus bars of width w_{bb}. One bus bar collects current from the back surface field (BSF) fingers; the other bus bar collects current from the emitter fingers. Isolation distance between metal contacts is w_i. Pitch *p* defines smallest repeating unit of back side cell structure.

Figures 2a-d illustrate the influence of *p* on η in Fig. 2a, *FF* in Fig. 2b, J_{SC} in Fig. 2c, and V_{OC} in Fig. 2d. The bars present the cells parameters for: A) an ideal case when the cell has no line resistance losses, and B) emitter- and BSF fingers having a resistivity ρ= 5 µΩcm that equals ρ of Ag screen printed paste. The fingers have a height h_f = 20 µm.

While both, J_{SC} and V_{OC} increase, the *FF* of the simulated cell decreases with increasing pitch *p*. Thus, the efficiency η first increases with increasing *p* due to the increase in J_{SC}, and V_{OC}, then reaches a maximal value, and then (because of the decrease in *FF*) η decreases by increasing *p*. Due to the metallization losses of case B, η and *FF* of the cell with metallization B are lower compared to case A. For the case A (the cell without line resistive losses), the fill factor decreases from FF_A = 81.9 % to FF_A = 78.2 % by increasing *p*. The efficiency shows a maximum efficiency $\eta_{A,max}$ = 24.9 % for *p* = 1000 µm, which drops to η_A = 24.4 % for *p* = 2000 µm. For case B (the cell with Ag screen printed fingers), the *FF* decreases from FF_B = 76.5 % to FF_B = 73.8 % by increasing *p*. The pitch size *p* = 1200 µm ($w_{f,em}$ = $w_{f,BSF}$ = 500 µm) provides a maximum $\eta_{B,max}$ = 23.4 % and drops to η_B = 23.0 % for a pitch *p* = 2000 µm .

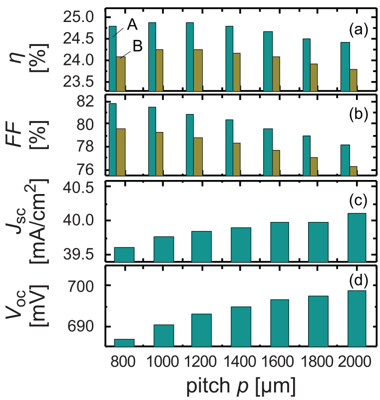

Figure 2:
Influence of pitch p on a) efficiency η, b) fill factor *FF*, c) short circuit current density J_{sc}, and c) open circuit voltage V_{oc} of the simulated BCBJ cell. Cell without finger line resistance is marked with A; cell with Ag screen printed fingers is marked with *B*. Depending on metallization, the efficiency η reaches a maximum at *p* = 1200 µm and $w_{f,em}$ = $w_{f,BSF}$ = 500 µm.

References:

[1] G. Kulushich, R. Zapf-Gottwick, A. Samadi, and J. H. Werner, *Proc. 27th EU PVSEC, 1272 (2012).*

Precise Carrier Concentration for Local Illumination

Author: P. Gedeon
In collaboration with: L. Stoicescu, M. B. Schubert, and J. H. Werner

For local illumination, the carrier diffusion length is usually larger than the illumination spot. In this case, the carrier concentration is calculated incorrect, when carrier diffusion is neglected. The neglect is typical for measurements with a small light spot scanned across the sample, such as microwave photo conductance decay. Hence, errors of several orders of magnitude occur in calculating the carrier concentration. Photoluminescence (PL) visualized the great extent of the carrier concentration reduction for small spots, as the PL intensity is proportional to the carrier concentration [1].

Figure 1 demonstrates our setup. A laser homogeneously illuminates a silicon wafer through a mask, creating a line focus. A camera captures the PL image. The line focus introduces a symmetric carrier distribution perpendicular to the focus.

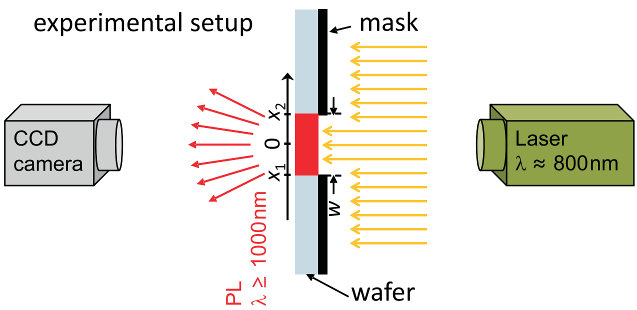

Figure 1:
Experimental setup for photoluminescence.

The solution of the continuity equation for spatially homogeneous illumination calculates the carrier concentration n from $n = G\tau$, with generation rate G and carrier lifetime τ [2]. This equation, however, neglects carrier diffusion. Figure 2 shows the PL intensity distribution perpendicular to the mask for different mask openings w. The maximum measured PL intensity Φ_{hom} represents spatially homogeneous laser illumination without a mask. For constant generation rate G, the signal reduces by up to three orders of magnitude when w becomes smaller than the carrier diffusion length L. In a first order approximation, our simulation calculates the local carrier concentration n from

$$n_{(x=0)} = G\tau \, \{1 - \exp(-w/2L)\} \qquad (1)$$

at the center $x = 0$ of illumination, depending on the mask opening w, and the carrier diffusion length L. Future work will concentrate on more precise models.

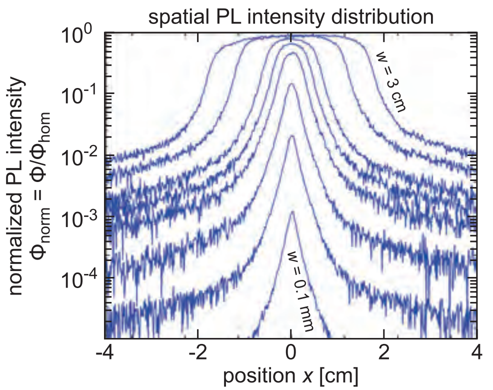

Figure 2:
PL intensity distribution perpendicular to mask openings in Figure1.

References:

[1] T. Trupke, R. A. Bardos, M. C. Schubert, and W. Warta, *Appl. Phys. Lett.* ***89****, 44107 (2006).*

[2] S. M. Sze and K. Ng. Kwok, *Physics of Semiconductor Devices, 3rd ed. (John Wiley & Sons, New Jersey, 2007), pp. 62-72.*

Daylight Luminescence for Photovoltaic System Testing

Author: L. Stoicescu
In collaboration with: M. Reuter and J. H. Werner

Day Light Luminescence System Testing (DaySy) provides electroluminescence (EL) and photoluminescence (PL) images of fully installed, operating photovoltaic (PV) modules and systems in bright daylight. This new method detects microcracks and inactive cell areas with high spatial resolution. DaySy pinpoint the exact nature of peculiar defects in any solar cell within a fully operational PV power plant.

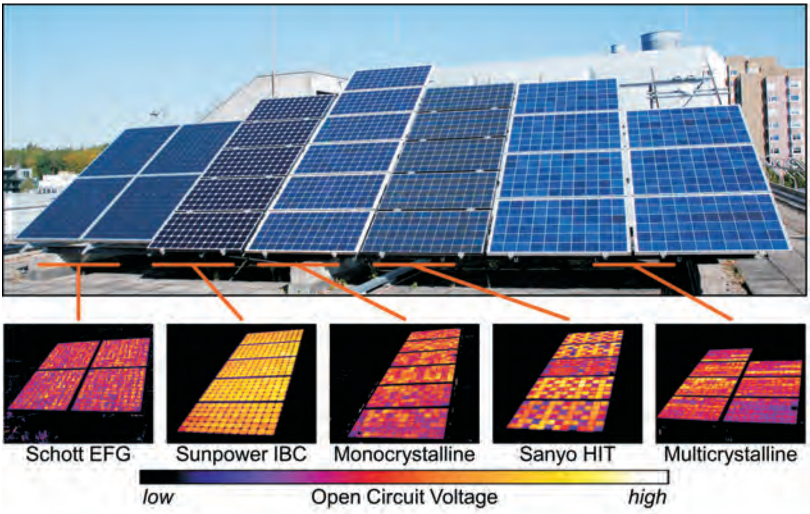

Figure 1:
DaySy measurements of the PV test systems installed at the University of Stuttgart. The top photograph shows five strings of different crystalline Si-technologies with 1 kW_p each. The lower part of the figure presents corresponding DaySy images of each string. In this case, the operating points of the PV generators are specifically chosen to create PL images, and each string is imaged separately. The open circuit voltage pattern delivered by the single solar cells of the system is clearly visible. Weak modules and low quality solar cells are instantly identified.

The quality of each image in Figs. 1, 2 depends on the acquisition time as well as on the luminescence intensity of the installed solar cells. On cell level, the EFG material is known to have low open circuit voltages of around 600 mV. Thus DaySy needed an acquisition time of 120 s. In contrast, for the Sanyo HIT modules only 5 s were necessary.

The advantage of our method lies in the ability to acquire luminescence images of complete PV power plants in bright daylight. Thus far we are able to identify cells with microcracks not visible with conventional thermography. Further work will identify potential induced degradation, snail tracks and broken fingers. In combination with thermography imaging [1, 2], DaySy will be capable to identify the exact nature of the defects in each defective solar cell of a PV power plant under normal operating conditions.

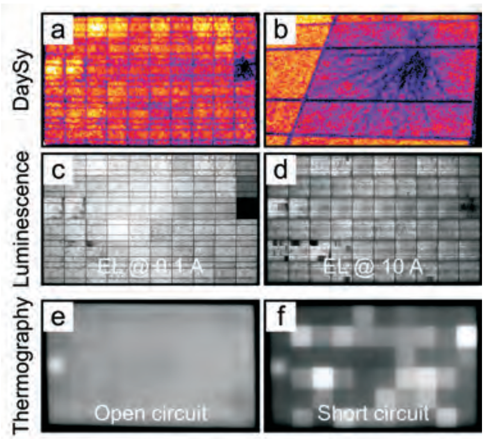

Figure 2:
(a,b) DaySy PL, (c,d) dark box EL, and (e,f) thermography. (b) A conspicuous solar cell displays a spider web of microcracks in the close-up. (c) The 0.1 A EL image exhibits a similar intensity distribution as the true PL DaySy image a). (d) Broken fingers visible in the 10 A high current EL image do not appear on the DaySy image a). The cracked cell in a) is not seen in thermography images (e,f).

References:

[1] R. Auer, U. Jahn, and C. Buerhop-Lutz, *Proc. 22nd EU PVSEC, 2519 (2007).*

[2] U. Hoyer, C. Buerhop, and U. Jahn, *Proc. 23rd EU PVSEC, 2913 (2008).*

19.4 % Efficient Laser Doped Back Contact Solar Cell

Author: M. Dahlinger
In collaboration with: B. Bazer-Bachi, T. C. Röder, R. Zapf-Gottwick, J. R. Köhler, and J. H. Werner

We present a fully laser doped interdigitated back contacted solar cell (IBC) with an efficiency η = 19.4 %. The high flexibility and spatial resolution of our process enables local n-type and p-type doping with a resolution below 30 µm without any masking.

Figure 1 presents the design and the process flow of the fully laser doped *ipv* IBC solar cell, starting with a one sided textured n-type silicon wafer. First, an optimized $POCl_3$ furnace diffusion [1] forms a lowly doped front surface field (FSF) on both sides of the wafer together with a phosphosilicate glass (PSG) layer. Subsequently, our *ipv* patented laser doping process irradiates the bulk contact area on the rear side of the wafer, forming deep and highly n^{++} doped regions using the phosphorus from the PSG. A 20 % KOH solution removes the non-irradiated n-type FSF regions on the rear side of the wafer, and a sputtering process deposits a thin boron precursor layer. A second laser doping process diffuses the boron locally into the wafer between the n-type regions forming the p^+-emitter. A 105 nm thermally grown silicon oxide layer serves as surface passivation and anti-reflective coating (ARC). Subsequently, evaporated Al and Ti/Pd/Ag layers contact the solar cell through the lithographically opened SiO_2.

The solar cells with an area A = 2×2 cm^2 are fabricated on a 4 inch n-type FZ wafer including busbars. Table I shows the results of the two best cells. At present (probably due to a contamination), our efficiency is limited to η = 19.4 %. Future work concentrates on avoiding this contamination.

Further optimization of the ARC, the passivation layer, the doping- and contact layout will enable us to boost the solar cell efficiency to 21 % and beyond. Future advanced solar cell concepts will also replace the photolithographic metallization by our laser transferred contact process [2].

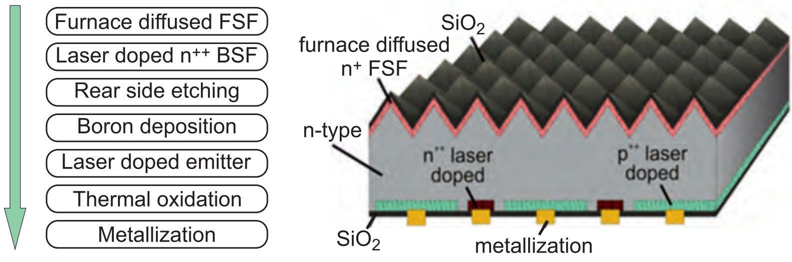

Figure 1:
Process flow and design of the *ipv* fully laser doped IBC solar cell. The n^{++} BSF as well as the p^{++} emitters are fabricated by laser doping without any masking.

Table I: Open circuit voltages V_{oc}, short circuit current density J_{sc}, fill factor *FF*, and efficiency η of first laser doped IBC cells.

	V_{oc} [mV]	J_{sc} [mA/cm^2]	*FF* [%]	η [%]
Cell 1	652	38.3	76.8	19.2*
Cell 2	661	39.1	75	19.4

*data independently confirmed.

References:

[1] B. Bazer-Bachi, P. Lill, M. Dahlinger, S. J. Eisele, R. Zapf-Gottwick, J. R. Köhler, and J. H. Werner, *Proc. 27th EU PVSEC*, 1954 (2012).

[2] E. Hoffmann, T. C. Röder, and J. R. Köhler, in *Proc. 38th IEEE Photovolt. Specialists Conf.* (IEEE, Piscataway, New York, 2012), in print.

Full Area Sb Laser Doped High Quality Emitters

Author: P. Lill
In collaboration with: M. Dahlinger and K. Carstens

This contribution presents Quasi Steady State Photo Conductance (QSSPC) evaluations of laser doped emitters using evaporated antimony as precursor. Polished float zone p-type silicon, with a base resistivity ρ_{base} = 3 Ωcm and a wafer thickness d_{wafer} = 275 µm is used as substrate. For the lifetime sample processing, hydrofluoric acid removes the native oxide from the silicon surface before Sb is deposited by thermal evaporation. Subsequently, the *ipv* laser doping process irradiates the samples with varied pulse energy density H_P on front and rear side to form a symmetrical emitter structure. After wet chemical cleaning, thermally grown silicon dioxide SiO_2 with subsequent forming gas annealing at T = 420 °C passivates the surface (as grown 80 nm SiO_2 are etched back to 25 nm). Supplementary to the SiO_2, low temperature Plasma Enhanced Chemical Vapor Deposition (PECVD) forms amorphous silicon (a-Si) as alternative passivation on additional lifetime samples.

Figure 1 shows the emitter saturation current density J_{0e} for sheet resistances R_{sh} between R_{sh} = 110 Ω/sq and R_{sh} = 150 Ω/sq of emitters created by varying precursor thickness and laser pulse energy density H_P. We extract the emitter saturation current density J_{0e} from QSSPC measurements of the effective minority carrier lifetime τ_{eff} with the method suggested by Cuevas et al. [1]. The very low emitter saturation current density below J_{0e} = 40 fA/cm^2 for samples passivated with a-Si demonstrates the high emitter quality of full area antimony laser doped emitters. Amorphous silicon passivation results in extremely low saturation currents 30 fA/cm^2 < J_{0e} < 40 fA/cm^2, indicating a defect free doping of the emitter. High temperature SiO_2 passivation yields emitter saturation current densities 90 fA/cm^2 < J_{0e} < 60 fA/cm^2 for emitter sheet resistances above R_{sh} = 110 Ω/sq. An optimized processing scheme regarding cleaning prior to the high temperature oxidation could possibly further improve the performance of the Sb emitters.

Assuming ideal diode characteristics and a short circuit current density J_{sc} = 35 mA/cm^2, which is achievable with full area laser doped solar cells [2], we calculate an upper open circuit voltage,

$$V_{oc,lim} = V_{therm} \ln\left(\frac{J_{sc}}{J_{0e}} + 1\right) \tag{1}$$

with the thermal voltage V_{th} = 25.7 mV. For a sheet resistance of R_{sh} = 114 Ω/sq, the measured emitter saturation current density J_{0e} = 65 fA/cm^2 yields an upper open circuit voltage limit V_{oc} = 694 mV, a number which shows the high quality of our Sb laser doped emitters.

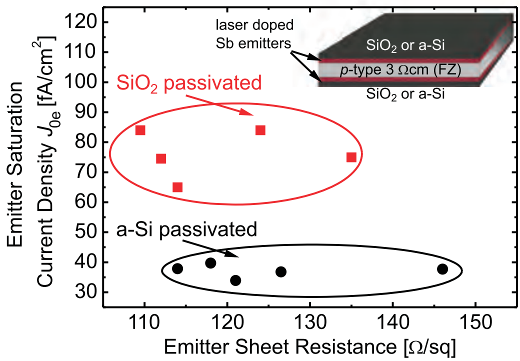

Figure 1:
Emitter saturation current densities of antimony laser doped n-type emitters, passivated with high temperature furnace oxidation or low temperature amorphous silicon. The inset shows the symmetrical structure of the lifetime samples, either passivated with 80 nm SiO_2 or with 74 nm a-Si.

References:

[1] R. A. Sinton, A. Cuevas, and M. Stuckings, *Proc. 25th IEEE Photovolt. Specialists Conf.* (IEEE, Piscataway, New York, 1996) pp. 457-460.

[2] M. Dahlinger, S. J. Eisele, J. R. Köhler, and J. H. Werner, *Proc. 26th EU PVSEC 1152* (2011).

Multi-Beam Optics for Laser Doped Selective Emitters

Author: T. C. Röder
In collaboration with: A. Bertram and J. R. Köhler

Our patented add-on selective laser doping process increases the doping concentration as well as the emitter depth underneath the contact fingers, thus yielding good ohmic contacts [1]. Selective laser doping does not only work in a research environment but is also compatible with industrial mass production and increases the cell efficiency up to 0.5 % (absolute). For industrial mass production, the selective laser doping has to be finished in less than one second. For this reason, in cooperation with different companies and research institutes, the *ipv* developed a multi-beam optics which enables a much faster selective laser doping.

Figure 1 shows the multi-beam optics, developed by the company LIMO. The set-up splits the incoming Gaussian laser beam of a newly developed 400 W Trumpf laser system into 17 single line shaped beams. The multi-beam optics enables a 17 times faster processing of selective emitter solar cells in comparison with a single laser beam. Table 1 shows the I/V-characteristics of first 156 cm^2 x 156 cm^2 monocrystalline selective emitter solar cells processed with the multi-beam optics. The emitter sheet resistance ρ_s between the contacts is ρ_s =117 Ω/sq. Depending on the laser power, the selective laser doping decreases the doping underneath the contact fingers down to 24 Ω/sq. The higher doping increases the fill factor FF = 76.3 % from the homogeneous doped cell to FF = 78.0 %. Additionally, the higher doping underneath the contacts shield the charge carriers from the contact interface which reduces the surface recombination and increases the open circuit voltage V_{oc} = 627 mV up to V_{oc} = 635 mV. Only the short circuit current density J_{sc} decreases with decreasing sheet resistance due to a deeper and longer melting of the silicon surface, reducing the performance of the surface texture.

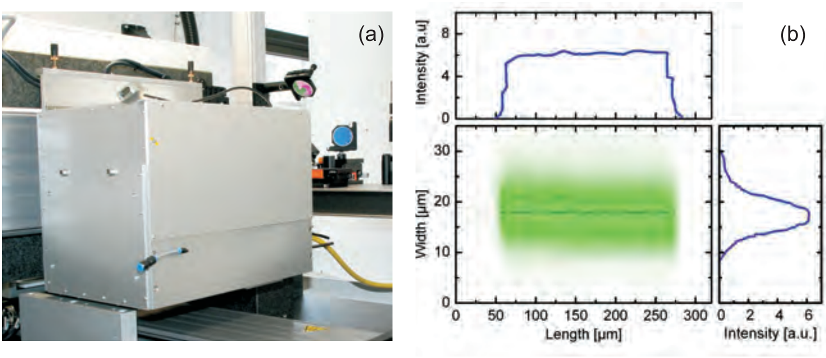

Figure 1:
(a) The LIMO multi-beam optics splits the laser beam into 17 single line shaped profiles.
(b) The profiles have a length l = 220 µm in the long and width w = 15 µm in the short axis.

Table I: I/V-characteristics of the best cells processed with the multi-beam optics in comparison with a cell without laser doping. The multi-beam optics increases the cell efficiency η by η = 0.6% absolute, mainly due to the low contact resistivity which increases the fill factor *FF*.

laser system	R_{sh} (contact) [Ω/sq]	*FF* [%]	J_{SC} [mA/cm^2]	V_{OC} [mV]	η [%]
Multi-beam	44	76.3	37.4	630	18.0
Multi-beam	30	77.5	37.2	633	18.2
Multi-beam	24	78.0	37.0	635	18.3
--	117	76.2	37.0	627	17.7

References:

[1] T. C. Röder, S. J. Eisele, P. Grabitz, C. Wagner, G. Kulushich, J. R. Köhler, and J. H. Werner, *Prog. Photovolt: Res. Appl.* ***18****, 505 - 510 (2010).*

Self-aligned Local Contacts Through a-Si:H Passivation Layer

Author: K. Carstens
In collaboration with: S. Miyajima and M. Schubert

We present a novel method forming less than 100 µm wide self-aligned local contacts through an amorphous silicon based passivation layer stack on p-type crystalline silicon solar cells.

Figure 1 shows the principle: wire shading during the plasma deposition with 100 µm wide wires, create a locally thinner intrinsic a-Si:H passivation layer. An amorphous silicon carbide layer (SiC_x) acts as a diffusion barrier for aluminum and prevents from Al-induced crystallization [1]. Evaporated Al forms local contacts to the p-type crystalline silicon during annealing at 350°C. No additional lithography or laser ablation is necessary for opening of the passivation layer.

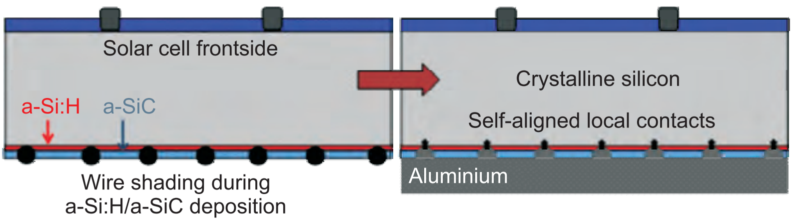

Figure 1:
Self-aligned local contacts through (i)a-Si:H passivation layer. Wire shading creates locally thinner deposition of an intrinsic a-Si:H passivation layer at the solar cell rear side. Evaporated aluminum forms local contacts during annealing. An amorphous silicon carbide layer acts as a diffusion barrier against aluminum

Figure 2 a) shows the contact formation during annealing at 350°C. Therefore, we use an Al/(p)c-Si/(i)a-Si (wire shaded)/SiC_x (wire shaded)/Al sample structure similar to Ref. [2] and measure the total resistance $R_{tot,500}$ from top to bottom.

A good ohmic contact $R_{tot,500}$< 0.5 W on a 2 x 2 cm^2 sample is achieved after about 80 min annealing time. Figure 2 b) confirms the temperature stability of the passivation layer during annealing and contact formation. Therefore, we use an (i)a-Si/(p)c-Si/ a-Si (wire shaded)/SiC_x (wire shaded)/Al sample structure and measure the relative implied open circuit voltage $V_{oc,imp,pl}$, by means of photoluminescence imaging during annealing. In addition, we determine the implied open circuit voltage $V_{oc,imp,qss}$ by QSSPC before deposition and after removal of the Al. Figure 2 b) shows a decrease of the implied open circuit voltage from $V_{oc,imp,qss}$= 730 mV to $V_{oc,imp,qss}$= 715 mV during annealing. These values correspond to a slight increase of the surface recombination velocity from S_{eff} = 15 cm/s to S_{eff} = 36 cm/s, or a slight to the widening of the local contacts from 20 µm to 100 µm during annealing.

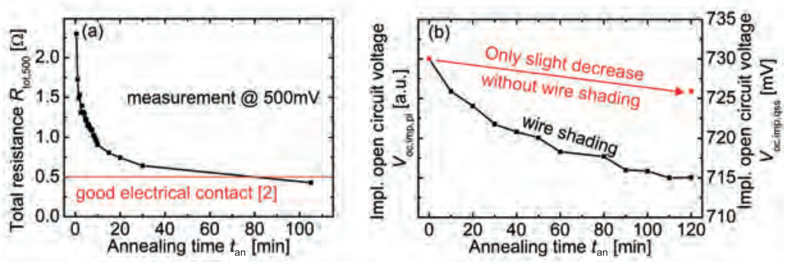

Figure 2:
a) A total resistance R_{tot} = 2 Wcm^2, necessary for a good rear side contact of a solar cell [9], is achieved after 80 min annealing time. **b)** During the annealing-time, the implied open circuit voltage reduces on a very high level by only about 15 mV.

In conclusion, we showed an elegant method to form less than 100 µm wide local ohmic contacts through an amorphous silicon based passivation layer for the rear side of p-type crystalline silicon solar cells with a low effective surface recombination velocity.

References:

[1] M. S.Haque, H. A. Naseem, and W. D. Brown, *J. Appl. Phys.* ***75,*** *3928 (1994).*

[2] E. Schneiderlöchner, Ph.D.Thesis (University of Freiburg, 2004), p. 80ff.

Optical Model for Luminescent Down-Shifting

Author: R. Rothemund

Luminescent down-shifting (LDS) is an elegant, purely optical method to improve the short-wavelength response of photovoltaic modules by red-shifting the incident solar spectrum [1]. This contribution presents a simple optical model to investigate luminescent down-shifting. The external quantum efficiency

$$EQE_{LDS}(\lambda) = f_{abs}(\lambda)\, \eta_{LDS}\, ESM + f_{trans}(\lambda)\, EQE_{ref}(\lambda) \qquad (1)$$

of a PV module with a LDS layer on top originates from absorbed ($0 \leq f_{abs}(\lambda) \leq 1$) and down-shifted photons, and from transmitted photons ($0 \leq f_{trans}(\lambda) \leq 1$). The LDS efficiency η_{LDS} quantifies the efficiency of the LDS layer to down-shift absorbed photons and send them towards the underlying solar cell. High emission spectral matching

$$ESM = \frac{\int PL(\lambda')\, EQE_{ref}(\lambda')d\lambda'}{\int PL(\lambda')d\lambda'} \qquad (2)$$

of the LDS emission spectrum $PL(\lambda)$ to $EQE_{ref}(\lambda)$ of the PV module ensures efficient conversion of down-shifted photons into charge carriers.

Figures 1a, b, and c show the excellent agreement between the optical model and the experimental *EQE* for a) mono-Si, b) multi-Si, and c) CdS/CdTe solar cells. Figure 2 presents LDS efficiencies extracted from fitting the experimental *EQE* and calculated *ESM* values. The upper limit indicated for η_{LDS} is valid for a photoluminescence quantum yield of 100 % and a photon escape cone loss of 12 %. For multi-Si and perylene-derivative dyes, LDS is close to its upper limit while LDS for CdS/CdTe shows great potential for improvement. Furthermore, it enables the screening of candidate LDS materials.

The presented optical model is fast, easy-to-use and universally applicable to analyze experimental LDS results. Furthermore, it enables the screening of candidate LDS materials.

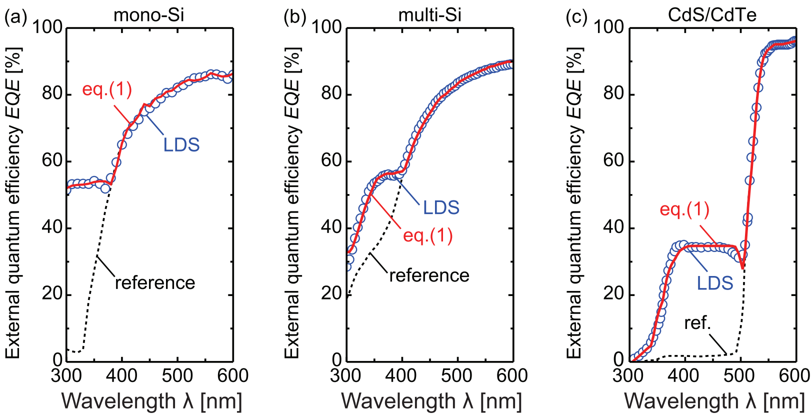

Figure 1:
The optical model shows excellent agreement with the experimental *EQE* for a) mono-Si, b) multi-Si, and c) CdS/CdTe solar cells.

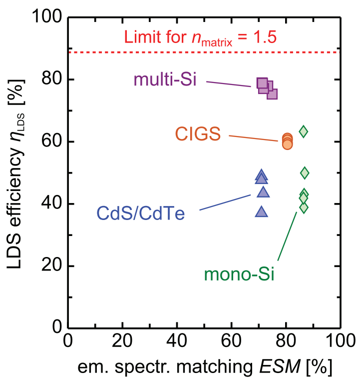

Figure 2:
LDS efficiency and emission spectral matching for various solar cell technologies and luminescent materials. The LDS efficiency is extracted from fitting the experimental *EQE* with the presented optical model.

References:

[1] E. Klampaftis, D. Ross, K. R. McIntosh and B. S. Richards, *Sol. En. Mat. Sol. Cells* **93**, 1182 (2009).

Internal and External Photoluminescence Spectra

Author: Jens Kistner

Most publications on photoluminescence (PL) present PL spectra that correspond to the spectral distribution $\Phi_{ext}(\lambda)$ of photons of wavelength λ measured outside the sample. However, $\Phi_{ext}(\lambda)$ differs in shape and intensity from the spectrum $\Phi_{int}(\lambda)$ generated inside the sample. In order to understand the origin of the PL, it is thus required to take a closer look at its emergence. Figure 1 sketches a simple model that allows for a more profound understanding of the PL. The discussed case assumes a reflective PL measurement. The homogeneous luminescent layer is described by the thickness d, the refractive index $n_1(\lambda)$, and the absorption coefficient $\alpha_1(\lambda)$. It is placed on a substrate with $n_2(\lambda)$ and $\alpha_2(\lambda)$. The sample is placed in air with $n_0(\lambda) = 1$ and $\alpha_0(\lambda) = 0$. The index "exc" allows to differentiate excitating photons at λ_{exc} from the ones generated by PL.

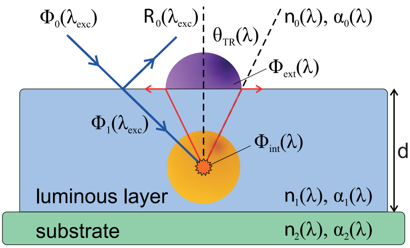

Figure 1:
Simplified model that describes the emergence of photoluminescence. Reflection and absorbance cause a reduction of the excitation $\Phi_0(\lambda_{exc})$. The generated internal spectrum $\Phi_{int}(\lambda)$ differs from the external spectrum $\Phi_{ext}(\lambda)$ due to wavelength dependent total reflection at the inner surface.

The PL setup excites the sample with the spectrum $\Phi_0(\lambda_{exc})$. However, not all of these photons are absorbed and generate luminescence inside the sample. The actual absorption spectrum

$$\Phi_1(\lambda_{exc}) = [1 - R_0(\lambda_{exc})]\left[1 - e^{-\alpha_1(\lambda_{exc})d}\right]\Phi_0(\lambda_{exc}) \tag{1}$$

depends on the external excitation $\Phi_0(\lambda_{exc})$, reflection losses $R_0(\lambda_{exc})$, and on the absorption coefficient $\alpha_1(\lambda_{exc})$ of the luminous layer. The absorbed photons $\Phi_1(\lambda_{exc})$ generate the internal PL spectrum $\Phi_{int}(\lambda)$. This process can be summarized by two parameters.

The transfer function $\Psi(\lambda_{exc}, \lambda)$ describes the spectral shift. The PL efficiency η_{PL} summarizes thereby occurring losses. In total, the actual PL process is described by

$$\Phi_{int}(\lambda) = \eta_{PL}\Psi(\lambda_{exc},\lambda)\Phi_1(\lambda_{exc}). \tag{2}$$

The model simplistically assumes an isotropic propagation of $\Phi_{int}(\lambda)$ with additional losses η_{rec} occuring due to recombination. Total reflection at the inner surface affects the external spectrum

$$\Phi_{ext}(\lambda) = \sin^2\left[\tfrac{1}{2}\arcsin\left(\tfrac{1}{n_1(\lambda)}\right)\right]\eta_{rec}\Phi_{int}(\lambda). \tag{3}$$

Due to the wavelength dependence of the refractive index, this transition may change the spatial distribution of the PL spectrum. Figures 2a and 2b illustrate the impact of the suggested model on the understanding of PL. Figure 2a applies Eq. (1) to different amorphous silicon suboxides. Depending on the oxygen content *x*, only a part of the initial excitation contributes to the generation of luminescence. Figure 2b clarifies the wavelength dependence of the internal and external PL according to Eq. (3). Only few of the generated photons emit out of the sample where they are detected. The example shows that omitting a correction according to Eq. (1) to (3) results in a misinterpretation of PL intensities and spectral weighting. Especially for the quantification of PL efficiencies and for comparative assertions these recalculations must be taken into account.

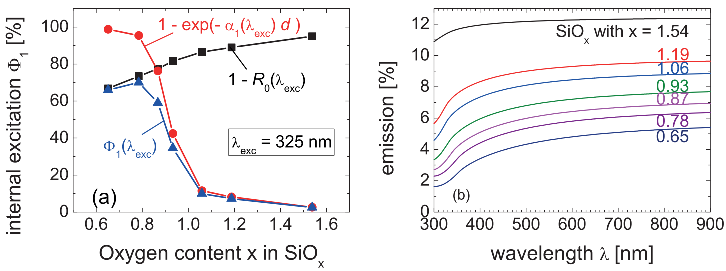

Figure 2:
Relevance of the model according to Fig. 1 for the PL of various silicon suboxides. a) Internal share $\Phi_1(\lambda_{exc})$ of the initial external excitation $\Phi_0(\lambda_{exc})$ that is absorbed in the luminous layer and thus contributes to the generation of PL (see Eq. (1)). b) External share $\Phi_{ext}(\lambda)$ of the generated PL $\Phi_{int}(\lambda)$ that is emitted (see Eq. (3)).

Hemispheric Intensity Distribution for Optimizing Light Trapping

Author: M. Berner
In collaboration with: M. Sämann, A. Garamoun, and M. B. Schubert*

A novel camera-based measurement setup enables the full quantification of the transmitted radiation deflected by structured front electrodes for thin film solar cells. The conventional measurement of the angular intensity distribution only analyzes one polar plane. The new hemispheric intensity distribution (HID) analysis quantifies the optical scattering and/or diffraction over the complete hemisphere. Figure 1 illustrates the basic setup of the camera-based HID measurement tool. A collimator, sourced by a fiber-coupled laser, irradiates the sample. The sample deflects the transmitted radiation of the collimated laser beam. To obtain the radiation's angular distribution in the transmission hemisphere, a plano-convex collecting lens follows the sample. Thereby, the direction of a deflected ray is described by the deflection angle α and the polar angle φ. The plano-convex lens transforms the angular distribution in the transmission hemisphere to a spatial distribution in the lens' focal plane, i.e. the plano-convex lens converts the incident radiation's direction to a position in the lens' focal plane.

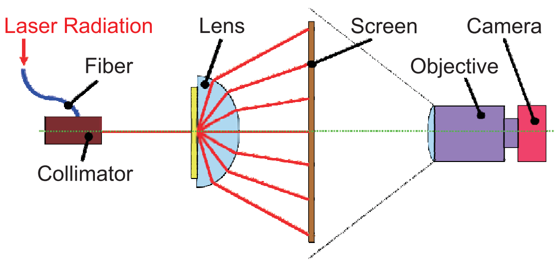

Figure 1:
Schematic view of the camera-based setup for hemispheric intensity distribution (HID) measurements. A collimated laser beam irradiates the sample. A collecting lens focuses the deflected transmitted radiation on the screen. The camera captures images of the intensity distribution from the screen.

**present address: ads-tec GmbH, Leinfelden-Echterdingen*

A screen images the distribution in the focal plane, and a 5-megapixel camera is used to capture the distribution on the screen. Only radiation deflected into angles $\alpha > 85°$ is not recorded due to experimental limitations.

Figure 2 shows a true-in-scale diagram of the angular intensity distribution of a thin film deflection structure at wavelength λ = 660 nm measured with the HID setup. The sample is a diffractive laser-structured ZnO:Al sample prepared at the *ipv*. The grey levels in the diagram represent the intensity in logarithmic scale of arbitrary units. Each concentric circle equates to one deflection angle α. The diagram clearly shows the different orders of diffraction by the laser-structured ZnO:Al.

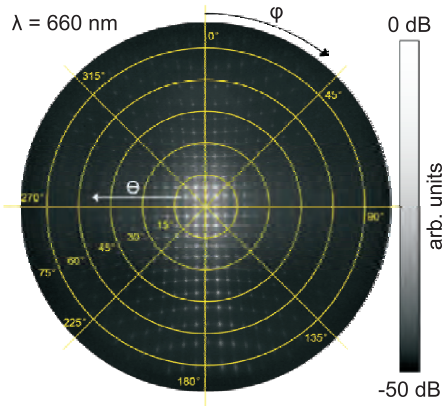

Figure 2:
Angular intensity distribution of a laser-structured diffractive grating on ZnO:Al, which is irradiated with wavelength λ = 660 nm.

Reference [1] gives a more detailed discussion of the *ipv* samples and the HID results, as well as a comparison of the *ipv* samples with Asahi® U-type SnO_2:F.

References:

[1] M. Berner, M. Sämann, A. Garamoun, and M. B. Schubert, *IEEE J. Photovoltaics* **99**, 1 (2012).

Publikationen
Publications

Optimizing P furnace Diffusion Layers for Laser Doping
B. Bazer-Bachi, P. Lill, M. Dahlinger, S. J. Eisele, R. Zapf-Gottwick, J. R. Köhler, and J. H. Werner, in *Proc. 27th Europ. Photovolt. Solar Energy Conf.*, (WIP, Munich, 2012), p. 1954

18.3 % Effciency on High Ohmic Emitters without Selective Emitters
B. Bazer-Bachi, G. Kulushich, T. Takahashi, H. Iida, R. Zapf-Gottwick, and J. H. Werner, Energy Procedia **27**, 531 - 536 (2012)

Quantification of Optical Deflection by Laser-Structured ZnO:Al
M. Berner, M. Sämann, A. Garamoun, and M. B. Schubert, *IEEE J. Photovoltaics* **99**, 1 (2012)

Self-aligned Local Contacts Through a-Si:H Passivation Layer
K. Carstens, S. Miyajima, and M. B. Schubert, Sol. Energy Mater. Sol. Cells **106**, 27 - 30 (2012)

µc-$Si_{1-x}C_x$:H Backside Passivation for Industrial Solar Cells
K. Carstens, S. Miyajima, R. Zapf-Gottwick, and M. B. Schubert, in *Proc. 4th Int. Forum on Multidisciplinary Educ. and Res. for Energy Science* (Tokyo Institute of Technology, Tokyo, 2011)

Highly Efficient Cu(In,Ga)Se_2 Solar Cells Grown on Flexible Polymer Films
A. Chirilă, S. Buecheler, F. Pianezzi, P. Bloesch, C. Gretener, A. R. Uhl, C. Fella, L. Kranz, J. Perrenoud, S. Seyrling, R. Verma, S. Nishiwaki, Y. E. Romanyuk, G. Bilger, and A. N. Tiwari, Nature Mater. **10**, 857 - 861 (2011)

+0.4% Efficiency Gain by Novel Texture for String Ribbon Solar Cells
J. Cichoszewski, M. Reuter, and J. H. Werner, Solar Energy Materials and Solar Cells **101**, 1 - 4 (2012)

Full-Area Laser-Doped Boron-Emitter Silicon Solar Cells
M. Dahlinger, S. J. Eisele, P. C. Lill, J. R. Köhler, and J. H. Werner, in *Proc. 38th IEEE Photovoltaic Specialist Conference*, (IEEE, New York, USA, 2012), pp. 1029 - 1031

19.2 % Laser doped Back Contact Solar Cell
M. Dahlinger, B. Bazer-Bachi, T. Röder, R. Zapf-Gottwick, J. R. Köhler, and J. H. Werner, in *Proc. 5th Int. Forum on Multidisciplinary Educ. and Res. for Energy Science* (Tokyo Institute of Technology, Tokyo, 2012)

Toward 6% in-situ Series Tandem a-Si/a-Si Module
A. Garamoun, R. Merz, S. Miyajima, and M. B. Schubert, in *Proc. 4th Int. Forum on Multidisciplinary Educ. and Res. for Energy Science* (Tokyo Institute of Technology, Tokyo, 2011)

Self-doping Laser Transferred Contacts for c-Si Solar Cells
E. Hoffmann, T. C. Röder, and J. R. Köhler, in *Proc. 38th IEEE Photovoltaic Specialist Conference*, (IEEE, New York, USA, 2012), pp. 1059 - 1062

Role of Phosphorus in Contact Formation on Silicon Solar Cells
G. Kulushich, R. Zapf-Gottwick, V. X. Nguyen, and J. H. Werner, Phys. Status Solidi Rapid Res. Lett. **6**, 370 - 372 (2012)

Contact Formation on 100 Ω/sq Emitter by Screen Printed Silver Paste
G. Kulushich, B. Bazer-Bachi, T. Takahashi, H. Iida, R. Zapf-Gottwick, and J. H. Werner, Energy Procedia **27**, 485 - 490 (2012)

Optimization of Laser Processed Back-Contacted Silicon Solar Cells
G. Kulushich, R. Zapf-Gottwick, A. Samadi, and J. H. Werner, in *Proc. 27th Europ. Photovolt. Solar Energy Conf.*, (WIP, Munich, 2012), p. 485

18.4 % Efficient Grid Optimized Cells with 100 Ω/sq Emitter
G. Kulushich, R. Zapf-Gottwick, B. Bazer-Bachi, and J. H. Werner, *IEEE J. Photovoltaics* xx, xxx (2012) (in press)

Laser Doping of Silicon using Antimony
P. C. Lill, M. Dahlinger, J. R. Köhler, and J. H. Werner, in *Proc. 27th Europ. Photovolt. Solar Energy Conf.*, (WIP, Munich, 2012), p. 1894

Full Area Antimony Laser Doped p-type Solar Cells
P. C. Lill, M. Dahlinger, J. R. Köhler, and J. H. Werner, in *Proc. 5th Int. Forum on Multidisciplinary Educ. and Res. for Energy Science* (Tokyo Institute of Technology, Tokyo, 2012)

Shunt Free Front and Back Contact Patterning During Roll-to-Roll Deposition
R. Merz, S. Miyajima, A. Madan, A. Garamoun, and M. B. Schubert, in *Proc. 26th Europ. Photovolt. Solar Energy Conf.* (WIP, Munich, 2011), p. 2731

Defect Formation in Silicon During Laser Doping
K. Ohmer, Y. Weng, J. R. Köhler, H. P. Strunk, and J. H. Werner, IEEE J. Photovoltaics **1**, 183 - 186 (2011)

Effect of Pulse Energy Density on Silicon during Laser Doping
K. Ohmer, Y. Weng, J. R. Köhler, H. P. Strunk, and J. H. Werner, in *Proc. 4th Int. Forum on Multidisciplinary Educ. and Res. for Energy Science* (Tokyo Institute of Technology, Tokyo, 2011)

Simulations of Geometry Effects and Loss Mechanisms Affecting the Photon Collection in Photovoltaic Fluorescent Collectors
L. Prönneke, G. C. Gläser, and U. Rau, EPJ Photovoltaics **3**, 30101, (2012), DOI : 10.1051/epjpv/2012001

Low Temperature Laser Metallization for Silicon Solar Cells
T. C. Röder, E. Hoffmann, B. Konrad, and J. R. Köhler, Energy Procedia **8**, 552 - 557 (2011)

Physical Model for the Laser Induced Forward Transfer Process
T. C. Röder and J. R. Köhler, Appl. Phys. Lett. **100**, 071603 (2012)

Laser Transferred Contacts: Modeling of the Transfer Process
T. C. Röder and J. R. Köhler, in *Proc. 38th IEEE Photovolt. Specialist Conf.* (IEEE, New York, USA, 2012), pp. 282 - 285

External Quantum Efficiency Analysis of Si Solar Cells with II-VI Nanocrystal Luminescent Downshifting Layers
R. Rothemund, S. Kreuzer, T. Umundum, G. Meinhardt, T. Fromherz, and W. Jantsch, Energy Procedia **10**, 83 - 87 (2011)

Light Trapping in Pyramidally Textured Crystalline Silicon Solar Cells Using Back-side Diffractive Gratings
R. Rothemund, T. Umundum, G. Meinhardt, K. Hingerl, T. Fromherz, and W. Jantsch, Prog. Photovolt: Res. Appl. (2012), DOI: 10.1002/pip.2192

Light trapping in Monocrystalline Si Solar Cells Using Back-side Diffraction Gratings
R. Rothemund, T. Umundum, G. Meinhardt, K. Hingerl, T. Fromherz, and W. Jantsch, Solid State Phenomena **178-179**, 446 - 450 (2011)

Time–resolved Photocurrent Measurements on PbS Nanocrystal Schottky–Contact Photovoltaic Cells.
R. Rothemund, S. Kreuzer, T. Fromherz, and W. Jantsch, Solid State Phenomena **178-179**, 56 - 60 (2011)

Full Area Simulation of Multicrystalline Silicon Solar Cells with High Spatial Resolution
L. Stoicescu, P. Gedeon, and G. C. Gläser, in *Proc. 37th IEEE Photovoltaic Specialist Conference*, (IEEE, New York, USA, 2011), p. 3495

Absolute Quantification of Gettering Efficiency from Luminescence Images
L. Stoicescu, M. Reuter and J. H. Werner, Energy Procedia **27**, 129 - 134 (2012)

Daylight Luminescence for Photovoltaic System Testing
L. Stoicescu, M. Reuter, and J. H. Werner, in *Proc. 22nd International Photovolt. Science and Engineering Conf.*, (Hangzhou, China, 2012), p. xx (in press)

Toxic Substances in Photovoltaic Modules
J. H. Werner, R. Zapf-Gottwick, M. Koch, and K. Fischer, in *Techn. Digest Intern. PVSEC-21 (Fukuoka, Japan, 2011),* Kennung: 3B-7O-06

Innovative Concepts for Solar Cells
J. H. Werner, M. Reuter, R. Zapf-Gottwick, J. R. Köhler, and M. Schubert, in *Proc. 4th Int. Forum on Multidisciplinary Educ. and Res. for Energy Science* (Tokyo Institute of Technology, Tokyo, 2011)

Arbeitsgemeinschaft
Cooperation Project

Steinbeiszentrum Photovoltaik

ipv

solar zentrum stuttgart

www.solarzentrum-stuttgart.com

Das Solarzentrum Stuttgart ist eine Arbeitsgemeinschaft des Institut für Photovoltaik (*ipv*) und des Steinbeiszentrum Photovoltaik (STZ-PV). Die Arbeitsgemeinschaft zielt auf eine noch engere Vernetzung der Forschung mit der industriellen Praxis.

Die Highlights 2012:

- Industrielle Umsetzung der metallunterstützten Textur in die Pilotproduktion bei der Sovello AG.
- Lumineszenzvermessung von PV-Systemen bei vollem Tageslicht (DaySy).
- Mobile Elektrolumineszenzmessung (MELI) von Photovoltaikmodulen.

Der Auftritt auf der europäischen Photovoltaikmesse EU PVSEC in Frankfurt war ein voller Erfolg: Der Stand des Solarzentrums war stets gut besucht. Auch die Teilnahme des Solarzentrums an der asiatischen Photovoltaikmesse in Hangzhou war ein weiterer Höhepunkt. Die enge Vernetzung mit der Grundlagenforschung und die industrielle Produktionserfahrung ermöglichen dem Solarzentrum die Charakterisierung, Beratung und Begutachtung von der Zellproduktion bis hin zum fertigen Photovoltaiksystem!

3

Lehrveranstaltungen
Lectures

Promotionen
Ph. D. Theses

Masterarbeiten
Master Theses

Bachelorarbeiten
Bachelor Theses

Gäste & ausländische Stipendiaten
Guests

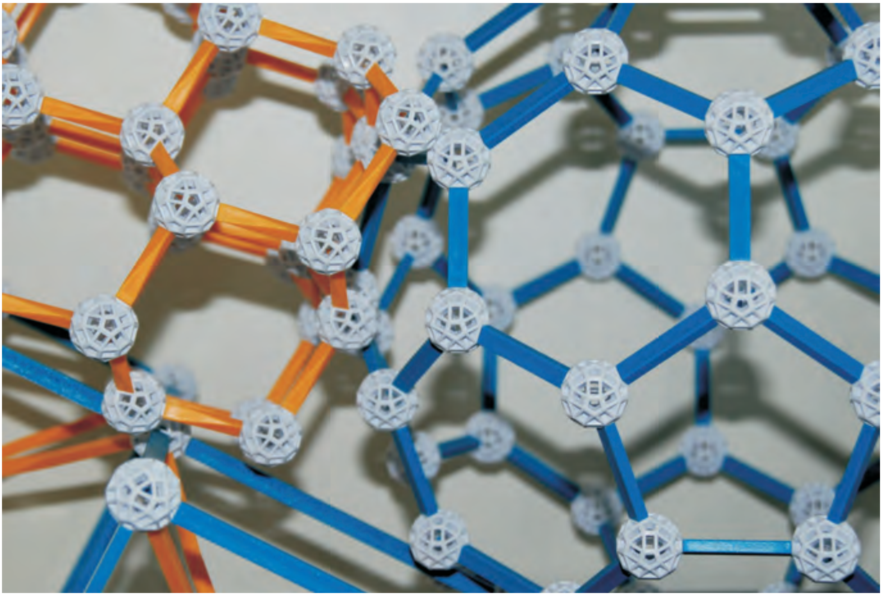

Mikroelektronik I (Bachelor, 1. Semester)

J. H. Werner

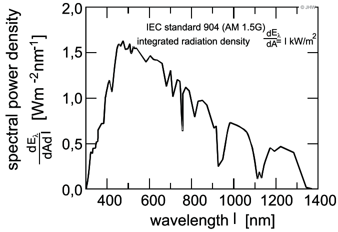

Energiebänder und Leitfähigkeit
Silizium - der Werkstoff der Mikroelektronik
Elektronen und Löcher in Halbleitern
Ströme in Halbleitern
Nichtgleichgewicht und Injektion
Elektrostatik des pn-Übergangs
Ströme im pn-Übergang

Energiewandlung (Master, 2. / 4. Semester)

J. H. Werner

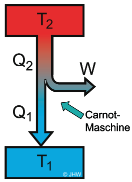

Grundlagen der Kernenergie
Thermodynamik
Direkte Nutzung der Sonnenenergie (Solarthermie, Photovoltaik)
Indirekte Nutzung der Sonnenenergie (Wasserkraft, Windenergie)
Chemische Wandlung und Speicherung elektrischer Energie

Laser and Light Sources (Master, 2. / 4. Semester)

J. H. Werner and J. R. Köhler

The Human Eye
Light and Color
Photometry
Incoherent Light Sources
Light Emitting Diodes
Lasers
Laser Processing

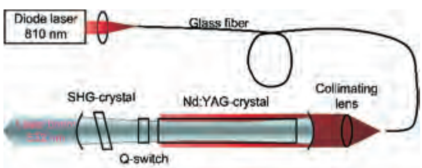

Optoelectronic Devices and Circuits I (Bachelor, 6. Semester)
J. H. Werner

Basic Physics
Thermal Radiation
Coherence
Semiconductor Basics
Excitation and Recombination Processes in Semiconductors
Light Emitting Diodes
Semiconductor Lasers
Glassfibers
Photodetectors

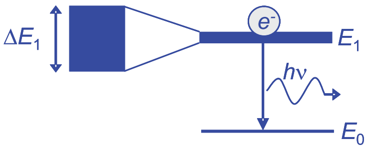

Photovoltaik I (Bachelor, 4. Semester)
J. H. Werner

Was die Photovoltaik leisten kann
Der Photovoltaische Effekt: Solarzelle, Solarmodul, Solaranlage
Sonnenspektrum und Energieverbrauch in Deutschland
Maximaler Wirkungsgrad einer Solarzelle
Grundprinzip einer Solarzelle
Ersatzschaltbild der Solarzelle
Photovoltaik-Materialien und -Technologien
Modultechnik
Photovoltaische Systemtechnik
Erträge von Photovoltaiksystemen
Photovoltaik-Markt

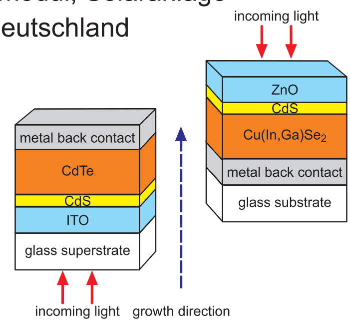

Photovoltaik II (Master, 1. / 3. Semester)
J. H. Werner

Technologie einkristalliner Zellen
Rekombinationsmechanismen
Theorie der maximalen Wirkungsgrade
Optimierungsstrategien
Zweite und Dritte Generation Photovoltaik

Festkörperelektronik (Master, 1. / 3. Semester)
J. H. Werner

Freie Elektronen als Teilchen und Wellen
Energiebänder in Festkörpern
Banddiagramme von Halbleitern
Ströme in Halbleitern
Emission von Elektronen aus Metallen und Halbleitern
Der Schottky-Kontakt
Photoeffekte in Halbleitern

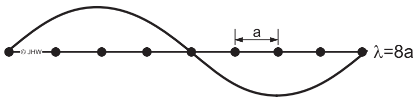

Wissenschaftliches Vortragen und Schreiben I (Wintersemester)
J. H. Werner

Kernbotschaften
Aufbau eines Vortrags
Standardfehler (Strukturfehler, Technikfehler, Fehler im Auftreten)
Praktische Schritte zum Vortrag
Selbst- und Fremdbeurteilung (mit Videoaufzeichung)

Wissenschaftliches Vortragen und Schreiben II (Sommersemester)
J. H. Werner

Kernbotschaften
Aufbau und Elemente einer Publikation
Bilder, Tabellen und Referenzen

Praktische Übungen im Labor „Halbleitermesstechnik“ (Master, 1. / 3. Semester)
J. H. Werner und M. B. Schubert

Herstellverfahren von Halbleitern und dünnen Schichten
Elektrische Messtechniken für Minoritäten und Majoritäten
Optische Messtechnik
Strukturelle Messtechniken

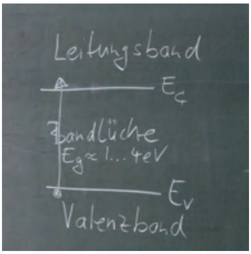
Leitungsband
Ec
Bandlücke
Eg ≈ 1...4eV
Ev
Valenzband


47.01 Hörsaal

Promotionen
Ph. D. Theses

Christian Ehling
Oberflächenpassivierung durch amorphes Silizium und amorphes Siliziumkarbid

Sebastian Eisele
Laserdotieren von Siliziumsolarzellen

Liv Prönneke
Fluorescent Materials for Silicon Solar Cells

Tobias Röder
Lasermetallisierung für Siliziumsolarzellen

Marc Sämann
Optimierung des Lichteinfangs von mikromorphen und einkristallinen Siliziumsolarzellen

Christian Ehling

Sebastian Eisele

Liv Prönneke

Tobias Röder

Marc Sämann

Masterarbeiten
Master Theses

Ke Chen
Tandemsolarzellen aus amorphem und nanokristallinem Silizium

Lejs Mersid Erden
Defektanalyse im Silizium

Ebrahim J. Gohari
Buried Contact Screen Printed Solar Cells

Imran Khan
Heavy Metal Free Pastes for Front Contacting Solar Cells

Stefan Koch
Charakterisierung lasertransferierter Kontakte
auf Siliziumsolarzellen

Ana Quilez Caballero
Temperature Profile Optimization of Industrial Firing Furnace
for Solar Cells

Fabian Rudnick
Lichtmanagement für Solarzellen und Solarmodule

Christian Sämann
Randintegrierte Bypassdioden für Siliziumsolarzellen

Jia Ye
Loss Analysis of Silicon Solar Cells during IPV Baseline Process

Bachelorarbeiten
Bachelor Theses

Alexander Birk
Gleichzeitige Messung der I/V-Kennlinie mehrerer Solarzellen

Markus Botey-Junca
Optimierung der Laserkantenisolation an kristallinen Solarzellen und Vergleich unterschiedlicher Positionen

Maria Eberspächer
Laserprozessierung und Charakterisierung von selektiven Emittern für Bifacial-Solarzellen

Timo Freund
Mobiler Elektrolumineszenz-Messplatz „MELi“

Michael Giek
Aufbau und Charakterisierung eines Modulflashers

Larsen Goder
Fluoreszenzkollektoren für fassadenintegrierte Photovoltaik

Felix Hantsch
Laserunterstützte Lötstellen

Helena Hingerl
Ausdiffusion von Bor aus flüssigem Silizium

Kordian Komarek
Sinterfähigkeit von Metallpasten unter Stickstoff

Tilman Müller
Laserinduzierte Aluminiumkontakte für c-Si-Solarzellen

Leander Rust
Optimierung von amorphen Passivierschichten für kristallines p-Typ Silizium

Matthias Schön
Kooptimierung des Rück- und Vorderseitenkontakts bei kristallinen Silizium-Solarzellen

Mehmed Taner
Automatische Erkennung von Defekten in Solarzellen

Lea Zeiner
Feinlinienmetallisierung über ein Zwei-Stufensieb

Andreas Zeuner
Laserepitaxie von Galliumphosphiddünnschichten

Gäste & ausländische Stipendiaten
Guests

Pedro Alpuim
Universidade do Minho, Guimarães, Portugal

Seyed Ali Mohammad Badri
Dalarna University, Falun, Schweden

Keelan Burns
Flinders University, Adelaide, Australien

Alex Fernando Borges Costa
Universidade Federal de São Carlos, São Carlos, Brasilien

Ebrahim Jamshidi Gohari
Dalarna University, Falun, Schweden

Maibi Malape
University of Fort Hare, Alice, Südafrika

Shinsuke Miyajima
Tokyo Institute of Technology, Tokyo, Japan

Jomar Julio Ruas
Pontifícia Universidade Católica de Minas Gerais, Brasilien

Satoshi Saijo
Nara Institute of Science and Technology, Nara, Japan

Aref Samadi
University of Teheran, Iran

Kousaku Shimizu
CIT Nihon University, Narashino Chiba, Japan

Yue-Shun Su
National Tsing Hua University, Taiwan

Was sonst noch war ...
More than Science ...

Mitarbeiterliste
Staff Members

Lageplan
Location Map

Was sonst noch war ...
More than Science ...

Tag der Wissenschaft

Am 30. Juni fand der diesjährige „Tag der Wissenschaft“ statt. Auch unser Institut nutzte die Gelegenheit, sich der interessierten Öffentlichkeit zu präsentieren und öffnete seine Türen. Neben Laborführungen und studentischen Vorführungen von selbstgebauten Energiewandlern konnte man sich auch ein Bild von der Tätigkeit des Solarzentrums machen.

Messeauftritt bei der EU PVSEC in Frankfurt/Main

Vom 25. bis 28. September präsentierte sich das *ipv* – innerhalb des Solarzentrum Stuttgart - mit einem Stand auf der EU PVSEC in Frankfurt/Main. Unser Messeauftritt zog viele Besucher an und bot neue Einblicke in die aktuelle wissenschaftliche Arbeit. Im Mittelpunkt der Aufmerksamkeit standen Live-Vorführungen von Elektrolumineszenzmessungen mittels Infrarotkamera zur Erkennung von Defekten an Solarmodulen (DaySy). Ausgestellt waren außerdem Prototypen aktueller Solarzellen, darunter komplett laserprozessierte Rückseitensolarzellen und Module mit neuartigen patentierten Lötverbindern.

Science Day

On 30$^{\text{th}}$ June the Science Day took place again. Our institute presented itself to the interested public and opened its doors. Everybody could get an idea of the work of the “Solarzentrum Stuttgart”. In addition to lab-tours, demonstrations of self-made power converters were shown by students.

A booth at the EU PVSEC in Frankfurt/Main

From September 25 to 28 the *ipv* presented itself - within the Solarzentrum Stuttgart - with a booth at the EU PVSEC in Frankfurt/Main. Our exhibition appearance attracted many visitors and offered new insights in the recent scientific work. The main focus of attention was on live demonstrations of electroluminescence measurements via an infrared camera to detect defects of solar modules (DaySy). Also presented were prototypes of current solar cells, including complete laser processed back contacted solar cells and modules with white painted cell connectors.


Solar-Tankstelle für E-Bikes
ipv
ipv

Installation Solartankstelle und Anschaffung E-Bike
Seit diesem Jahr können wir stolz behaupten, eine institutseigene Solartankstelle für E-Bikes zu besitzen. Somit bieten wir die Möglichkeit, E-Bikes umweltfreundlich und kostenlos aufzuladen. Seit Kurzem rundet nun auch der Besitz eines eigenen E-Bikes, welches von den Mitarbeitern genutzt werden kann, unser Angebot ab.

Grillfest mit der Fachschaft
Bei angenehmen sommerlichen Temperaturen fand im Juni das gemeinsame Grillen des *ipv* mit der Fachschaft Elektrotechnik auf dem Rasen vor dem Institutsgebäude statt. Der Abend war eine gute Gelegenheit, um sich in zwangloser Runde auszutauschen.

Energie-Preis der Otto F. Scharr-Stiftung
Sebastian Eisele bekam für seine Dissertation zum Thema „Laserdotieren von Siliziumsolarzellen" von der Otto F. Scharr-Stiftung den 1. Preis verliehen. Er nahm die Auszeichnung im Rahmen einer Festveranstaltung entgegen.

Installing solar station and purchase E-bike
Since this year we can proudly claim to have an institute's own solar charging station for electric bikes. Thus, we offer the opportunity to change E-bikes environmentally friendly and free. Recently, we aquired also an own E-bike, which is used by our employees.

Barbecue with the student council
At pleasant summer temperatures in June the barbecue of the *ipv* together with the student council of Electrical Engineering took place on the lawn in front of the institute building. The evening was an opportunity to exchange views and to discuss in an informal round.

Energy Award by the Otto F. Scharr-Foundation
With his Ph.D. thesis on "Laserdoping of Silicon Solar Cells" Sebastian Eisele got the first prize by the Otto F. Scharr-Foundation. He received this award at a ceremonial session.

Mitarbeiterliste

Staff Members

Name	Telefon 0711 - 685 - ...	E-Mail (vorname.name @ipv.uni-stuttgart.de)	Arbeitsgebiet
Leo Bauer	60105	leo.bauer	Technologie-Support
Barbara Bazer-Bachi	67160	barbara.bazer-bachi	Industrielle Solarzellen
Lydia Beisel	67169	lydia.beisel	Technologie-Support
Marcel Berner	67198	marcel.berner	Systemtechnik
Alexander Bertram	67163	alexander.bertram	Laserbearbeitung
Kai Carstens	67161	kai.carstens	Silizium-Heterostrukturen
Morris Dahlinger	67179	morris.dahlinger	Laserdotieren
Ahmed Garamoun	67181	ahmed.garamoun	Dünnschicht-Silizium, Tandemzellen
Panagiotis Gedeon	67182	panagiotis.gedeon	Messtechnik

Lars Hamann	69217	lars.hamann	Modultechnologie, Metallisierung
Anja Hardekopf	67268	anja.hardekopf	Öffentlichkeitsarbeit
Erika Herrera Calderon	67184	erika.herreracalderon	Industrielle Solarzellen
Freymut Hilscher	67141	freymut.hilscher	Sekretariat
Erik Hoffmann	60106	erik.hoffmann	Laser-induzierte Metallisierung
Hermann Hörth	67158	hermann.hoerth	Buchhaltung
Irmgard Kerschbaum	67158	irmgard.kerschbaum	Buchhaltung
Isabel Kessler	67141	isabel.kessler	Sekretariat
Jens Kistner	69223	jens.kistner	Dünnschicht-Silizium, Lumineszenz
Gordana Kulushich	69218	gordana.kulushich	Modellierung
Jürgen Köhler	67159	juergen.koehler	Laserprozesse, Verwaltung

Patrick Lill	67171	patrick.lill	Laserdotieren
Brigitte Lutz	67200	brigitte.lutz	Technologie-Support
Hendrik Moldenhauer	67142	hendrik.moldenhauer	Technologie-Support
Kathrin Ohmer	69216	kathrin.ohmer	Laserdotieren
Liv Prönneke	69214	liv.proenneke	Optik von Solarzellen
Anton Riß	67214	anton.riss	Werkstatt
Ralph Rothemund	67178	ralph.rothemund	Optik von Solarzellen
Tobias Röder	69213	tobias.roeder	Laser-induzierte Metallisierung
Matthias Saueressig	67180	matthias.saueressig	Siebdrucktechnologie
Markus Schubert	67145	markus.schubert	Stellv. Institutsleiter, Dünnschicht-Silizium, Charakterisierung
Liviu Stoicescu	67245	liviu.stoicescu	Optische Charakterisierung

Sergej Vollmer	67201	sergej.vollmer	Technologie-Support
Jürgen Werner	67140	juergen.werner	Institutsleiter, Leitung Forschung, Lehre, Verwaltung
Birgitt Winter	67162	birgitt.winter	Technologie-Support
Thomas Wurster	67246	thomas.wurster	Systemtechnik
Renate Zapf-Gottwick	69225	renate.zapf-gottwick	Industrielle Solarzellen

Lageplan
Location Plan

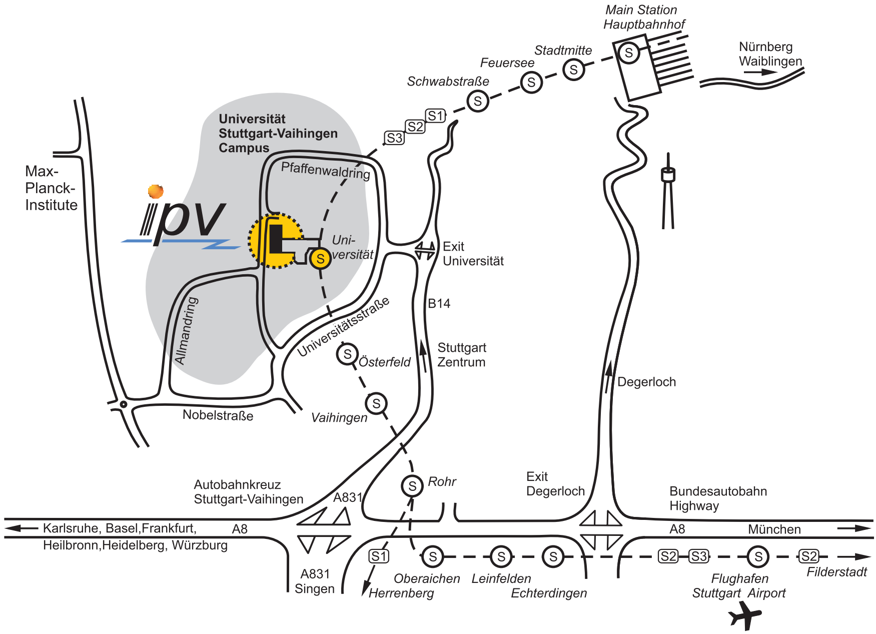

Institut für Photovoltaik
Pfaffenwaldring 47
70569 Stuttgart

Tel.: 0711 / 685-67141

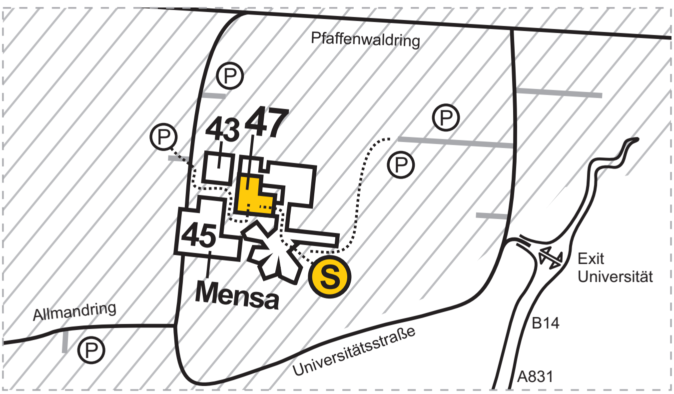

Institut für Photovoltaik
Universität Stuttgart

Pfaffenwaldring 47
70569 Stuttgart

Phone: +49 711 685 67141
FAX: +49 711 685 67143

www.ipv.uni-stuttgart.de